Rapid solidification synthesis of novel (La,Y)2(Zr,Ti)2O7 pyrochlore-based glass-ceramics for the immobilization of high-level wastes

Yongchang Guo, Ying Zhang, Mathieu Allix, Shaowei Feng, Hong Sun, Cécile Genevois, Emmanuel Véron, Jianqiang Li

Rapid solidification synthesis of novel $(La,Y)_2(Zr,Ti)_2O_7$ pyrochlore-based glass-ceramics for the immobilization of high-level wastes

Yongchang Guo[a,b], Ying Zhang[a,b], Mathieu Allix[d*], Shaowei Feng[a,b], Hong Sun[a,b], Cécile Genevois[d], Emmanuel Véron[d], Jianqiang Li[a,b,c*]

[a] CAS Key Laboratory of Green Process and Engineering, National Engineering Laboratory for Hydrometallurgical Cleaner Production Technology, Institute of Process Engineering, Chinese Academy of Sciences, Beijing 100190, P. R. China.

[b] University of Chinese Academy of Sciences, Beijing 100049, P. R. China.

[c] Innovation Academy for Green Manufacture, Chinese Academy of Sciences, Beijing 100190, P. R. China.

[d] CNRS, CEMHTI UPR 3079, Univ. Orléans, F-45071 Orléans, France.

*Correspondence: E-mail address: jqli@ipe.ac.cn, mathieu.allix@cnrs-orleans.fr

Abstract

Pyrochlore-based glass-ceramics are attracting attention as a promising host material for immobilizing minor actinide in high-level wastes. However, the loading capacity of pyrochlore-based materials for actinide elements is to be improved, and only conventional synthetic approaches of powder sintering and glassy bulk crystallization were reported. Here, new $(La,Y)_2(Zr,Ti)_2O_7$ pyrochlore-based glass-ceramics were subtly designed and successfully prepared through a rapid melting and solidification process. The solidification behavior of samples with different cooling rates was investigated, the dense and crack-free $(La,Y)_2(Zr,Ti)_2O_7$ pyrochlore-based glass-ceramics were prepared at the cooling rate of 500 ˚C/s (within 1.5 s). The present amorphous La_2O_3-TiO_2-Al_2O_3 phase demonstrates the outstanding thermal stability compared with the currently used borosilicate glass for high-level waste immobilization due to the lack of conventional glass-forming components. The results show the great feasibility of this novel synthesis route for glass-ceramics by direct solidification and its good potential for immobilizing high-level wastes.

Keywords

Melt solidification, Pyrochlore glass-ceramics, Actinide immobilization, High-level wastes, Metastable crystalline phase

1. Introduction

High-level wastes (HLWs) generated by the reprocessing of spent nuclear fuels (SNFs) from nuclear facilities contain a large amount of radioactive elements. Transuranium minor actinides based nuclear wastes have long half-life and it is urgent to find suitable ways to store them in a stable and durable form [1-3]. At present, a variety of materials and techniques are available for the immobilization of high-level wastes (HLWs), including vitrification, crystallization into ceramics and the combination of both in a glass-ceramics system [4-6]. Glass possesses extraordinary loading capacity for various wasted nuclides and has the advantage of relatively simple and mature preparation process, which is the mainstream method of the immobilization of high-level wastes in industry [7]. However, confined by the poor chemical stability and radiation tolerance owing to its metastable nature, coupled with the low solubility of minor actinides, glass immobilization remains challenging for long-term and stable HLWs storage [8]. In comparison, ceramics exhibit long-term chemical stability and high minor actinides loading due to the localization of actinides in specific crystallographic sites in lattices [9]. Nevertheless, the rigorous selection of elements and limitation of ceramic crystal structures result in difficulties of ceramics immobilization to practical application [10-11]. Therefore, in recent years, glass-ceramics are attracting much attention as a promising host material for minor actinide immobilization because it can combine the advantages of glass and ceramics, meanwhile, supplement their shortcomings [12-14].

Currently, glass-ceramics with various crystalline structures have been investigated for the immobilization of high-level wastes (HLWs), including perovskite [15], pyrochlore [16-22], zirconolite [14,23-24] and brannerite [18,19,25]. Among these, the pyrochlore structure offers a wide range of possibilities for the immobilization of actinide nuclides due to the flexibility of the $A_2B_2O_7$ structure, in which A, B and O are 8-, 6- and 4-coordinated cation sites, respectively [9,26-29]. Additionally, reports on radiation damage have revealed that the chemical stability of the pyrochlore structure is sustained even in the completely amorphous states [30,31]. Current research on pyrochlore-based glass-ceramics are mainly focused on compositions considering a single element on the B site, such as titanate pyrochlore ($A_2Ti_2O_7$) and zirconite pyrochlore ($A_2Zr_2O_7$) [4,9,32-33]. Previous reports showed that the $A_2B_2O_7$ pyrochlore structure is stable only when the A/B ionic radii ratio is in the range of 1.46-1.78, otherwise the defect fluorite structure or

monoclinic structure are likely to be stabilized [34]. The current consideration of B-site occupation by a single element is limiting the application of pyrochlore-structured glass-ceramics to immobilize diverse actinide nuclides. Therefore, binary, or even multiple elements occupation on the B-site of pyrochlore-based glass-ceramics with subtle differences in ionic radii are expected to improve the loading flexibility of actinide nuclides, while sustained high loading capacity. In this work, possibility and feasibility of synthesizing binary substituted $(La,Y)_2(Zr,Ti)_2O_7$ pyrochlore-based glass-ceramics were investigated.

The possibility of industrial production of materials ensuring the immobilization of high-level wastes (HLWs) depends not only on the nature of the host materials but also on the complexity of the process. Currently, there are two primary processes to synthesize pyrochlore-based glass-ceramics. The first approach consists in sintering a mixture of borosilicate glass and crystalline pyrochlore powders, in which the glass powder is obtained by classic melt-quenching process followed by fine grinding while the crystalline pyrochlore powder is usually prepared by solid-state reaction process or sol-gel route [35-37]. The second approach to synthesis pyrochlore-based glass-ceramics is based on the controlled crystallization of a glass precursor bulk [14,16,22]. Both the sintering and crystallization methods were widely studied and show various advantages in the immobilization of high-level wastes (HLWs). However, the complexity of the processes has limited their development at the industrial application. Recently, Xirui Lu et al. reported a method of rapid in situ synthesis of $Gd_2Zr_2O_7$ glass-ceramics using spark plasma sintering [38], which greatly simplifies the synthesis process while increasing the preparation speed compared with the conventional sintering method and crystallization methods. However, the pressure required (30 MPa) during the sintering process and the existence of cracks at the surface of the obtained $Gd_2Zr_2O_7$ glass-ceramics also limit the industrial application and still require further improvement. Melt solidification is widely used in the synthesis of metals and alloys, which exhibits the advantages of brief and rapid process. Additionally, dense and crack-free solids are expected to be obtained during solidification owing to the good fluidity of the sample melts, and there may be novel glass-ceramic structures discovered due to the rapid melt solidification and crystal growth. However, the preparation of pyrochlore-based glass-ceramics for the immobilization of high-level wastes in this way has never been reported so far.

Aerodynamic levitation (ADL) was extensively used in the fabrication of novel/metastable

materials [39-41]. This synthesis process possesses the advantages of high heating power, no contact and no heterogeneous crystallization, high quenching rate which provides access to metastable phases. Additionally, the samples are levitated and the whole process avoids any contact with the wall of container, which confirm with the simple and the pollution-free demand of the immobilization of high-level wastes (HLWs). In this work, we demonstrate the rapid solidification synthesis of novel $(La,Y)_2(Zr,Ti)_2O_7$ pyrochlore-based glass-ceramics by aerodynamic levitation (ADL) process. The different cooling rates during solidification and the corresponding phase evolution of samples were investigated. The $(La,Y)_2(Zr,Ti)_2O_7$ pyrochlore-based glass-ceramics were successfully synthesized at the cooling rate of 500 ˚C/s (within 1.5 s). Results demonstrate that the prepared glass-ceramics were dense and crack-free, possess excellent thermal stability, and therefore have promising applications in nuclear waste disposal. Additionally, the successful synthesis of $(La,Y)_2(Zr,Ti)_2O_7$ pyrochlore-based glass-ceramics appears as a promising alternative for the immobilization of HLWs, with simplified preparation process and easier industrial production.

2. Material and Methods

2.1 Sample preparation

Samples were elaborated by aerodynamic levitator (ADL). The high purity oxide powders La_2O_3, TiO_2, Y_2O_3 and ZrO_2, Al_2O_3 in 99.99% purity were purchased from Sinopharm chemical reagent co. ltd and Aladdin chemical reagent co. ltd, respectively. All raw material powders were heated at 1000 ˚C in a muffle furnace for at least 2 h to remove adsorbed water. Then the raw materials were weighed and mixed stoichiometrically with the nominal composition of La_2O_3-Y_2O_3-2TiO_2-2ZrO_2-Al_2O_3 in molar ratio. The mixed powders were subsequently ground with ethanol and dry thoroughly in the oven. The obtained dried precursor was then pressed into pellets and crumbled into small pieces. Prior to melts, all pieces were pre-sintered at 600 ˚C for 2 h in air to obtain higher strength. Pieces of ~60-200 mg were then levitated on the nozzle of an ADL with oxygen flow and heated to melt (~2200 ˚C) by three CO_2 lasers. Keeping the molten state of samples for 10~20 s to ensure that the components were homogeneously distributed, then adjusting the laser power to solidify the melt via different cooling rates and the white and spherical samples were obtained. The ADL and the solidification process of samples are presented in Figure 1.

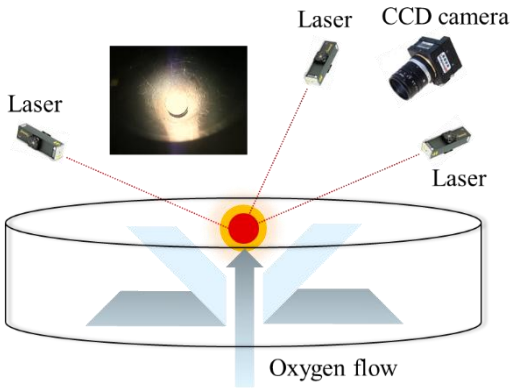

Figure 1. Schematic diagram of the aerodynamic levitator (ADL) with laser heating and the insert showed the $(La,Y)_2(Zr,Ti)_2O_7$ pyrochlore-based glass-ceramics melt.

2.2 Characterization

The solidification cooling curves were obtained from the data acquisition system of aerodynamic levitator with infrared pyrometer (FTK9S-P400A-20S11-0549, JAPANSENSOR Corporation, Tokyo, Japan). The structure of the obtained $(La,Y)_2(Zr,Ti)_2O_7$ pyrochlore-based glass-ceramics were identified by X-ray powder diffraction (XRPD, Smartlab 9, Rigaku Corporation, Tokyo, Japan). The surface morphology and elements distribution of samples were analyzed by the Field Emission Scanning Electron Microscope (FE-SEM, JSM-7610F, Tokyo, Japan) with energy dispersive spectroscopy (EDS). Prior to SEM observation, the bead samples were pre-processing in advance such as polishing and ion thinning treatment. The accelerating voltage and probe current of SEM were 15 kV and 8, respectively. The nanostructure of $(La,Y)_2(Zr,Ti)_2O_7$ pyrochlore-based glass-ceramics were observed by Transmission Electron Microscopy (TEM), using a JEOL ARM 200F (JEOL Ltd.) Cold FEG microscope operating at 200kV, equipped with a double spherical aberration correctors and fitted with a JEOL SDD CENTURIO EDS system. Bright-field (BF) and High Resolution TEM (HRTEM) images were recorded with a parallel beam. In addition, Scanning TEM – High Angle Annular Dark Field (STEM-HAADF) imaging, with a 68-174.5 mrad inner-outer collection angles, and STEM-EDS elemental mapping were performed with a probe size of 0.13nm. Prior TEM observations, the sample was crushed in ethanol, and a drop of the solution containing a small amount of material in suspension was deposited onto a carbon-coated copper grid. The glass transition temperature T_g was measured by a differential scanning calorimeter (Differential thermal analysis (DTA), STA499F3, NETZSCH, Selb, Germany) from room temperature to 1200 ˚C at a heating rate of 10

˚C/min in Ar atmosphere.

3. Results and discussion

The solidification cooling curves of the as-synthesized $(La,Y)_2(Zr,Ti)_2O_7$ pyrochlore-based glass-ceramics at different cooling rates were shown in Figure 2(a), the method used to calculated the cooling rate is presented in Figure 2(b) and the inset picture showed the resulting bead samples. The cooling rates refer to the cooling from the melt (~2200 ˚C) down to melt solidification (~1500 ˚C), which could be set and automatically controlled by the temperature control system of the aerodynamic levitator via adjustment of the laser power. The cooling rates were set to 100 ˚C/s, 130 ˚C/s, 200 ˚C/s, 300 ˚C/s and 500 ˚C/s (free cooling), respectively. In Figure 2(a), all samples were first heated up to melting (~2200 ˚C) and the recalescence peaks were observed during the cooling process, which indicated that the melt crystallized during solidification. The observed recalescence peaks at about 1500 ˚C are related to the main phase crystallization. Additionally, the recalescence peak temperatures vary with the cooling rate. Very tiny peaks were observed at about 1500 ˚C when the cooling rate was 500 ˚C/s (free cooling), 300 ˚C/s and 200 ˚C/s, respectively. With the decrease of the cooling rate to 130 ˚C/s and 100 ˚C/s, the recalescence peaks became stronger and show a slightly up shift. The enhancement of recalescence peaks with the decrease of cooling rate was due to the higher crystallinity of the main crystal phase under the lower solidification cooling rates. The slightly down shifted recalescence peaks with the increased cooling rate could be owing to the solidification point depression caused by deep supercooling. Particularly, the second recalescence peaks were observed when the cooling rate was ≤ 138 ˚C/s, which was related to the secondary crystallization of residual amorphous phase.

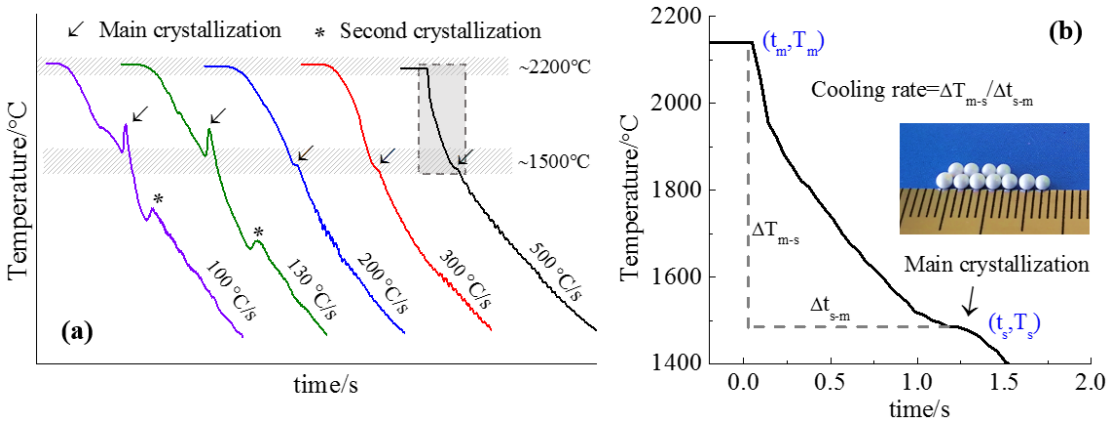

Figure 2. Cooling curves of samples during melt solidification. (a) Temperature-time profiles of

the solidified $(La,Y)_2(Zr,Ti)_2O_7$ pyrochlore-based glass-ceramics at different cooling rates, (b) the enlargement of temperature-time patterns in the gray dotted area exhibits the method used to define the cooling rate (the insert showed the prepared bead samples at a maximum cooling rate of 500 ˚C/s). The average cooling rates were 100 ˚C/s, 130 ˚C/s, 200 ˚C/s, 300 ˚C/s and 500 ˚C/s (free cooling), respectively.

The XRPD patterns of the as-synthesized $(La,Y)_2(Zr,Ti)_2O_7$ pyrochlore-based glass-ceramics synthesized at different cooling rates are shown in Figure 3(a). All samples match well with the standard card of $Y_2Zr_2O_7$ (pyrochlore 04-001-9350) which indicating that the crystalline phase in the obtained samples were pyrochlore. Additionally, a secondary phase appears and the $La_{0.9}Ti_{0.466}Al_{0.465}O_{2.9}$ (perovskite 04-009-2737) is observed (see for example the peak at 2θ=33°) with the decrease of the cooling rate to 130 ˚C/s, which is consistent with the analysis of solidification cooling curves showing a second recalescence peak. For better analysis of the phase evolution of the second crystallization, the XRPD patterns of the as-synthesized $(La,Y)_2(Zr,Ti)_2O_7$ pyrochlore-based glass-ceramics at different cooling rates were enlarged between 30° and 36°, as presented Figure 3(b). It can be observed that the diffraction peak intensity of 2θ=33° appears negligible when the cooling rate is 500 ˚C/s (free cooling) and slightly increased while the cooling rate is decreased to 300 ˚C/s and 200 ˚C/s. Particularly, with the decrease of the cooling rate to 130 ˚C/s and 100 ˚C/s, a significant enhancement of the diffraction peak intensity of the secondary phase was detected, which indicates that a relatively low cooling rate was unfavorable to the preparation of $(La,Y)_2(Zr,Ti)_2O_7$ pyrochlore-based glass-ceramics. The formation of the secondary phase seems related to the slow crystallization of the remaining glass. The reduced cooling rate provides more time for atomic rearrangement and crystallization of $La_{0.9}Ti_{0.466}Al_{0.465}O_{2.9}$ in the residual amorphous phase. Therefore, increasing the cooling rate is conducive to obtaining ideal $(La,Y)_2(Zr,Ti)_2O_7$ pyrochlore-based glass-ceramics.

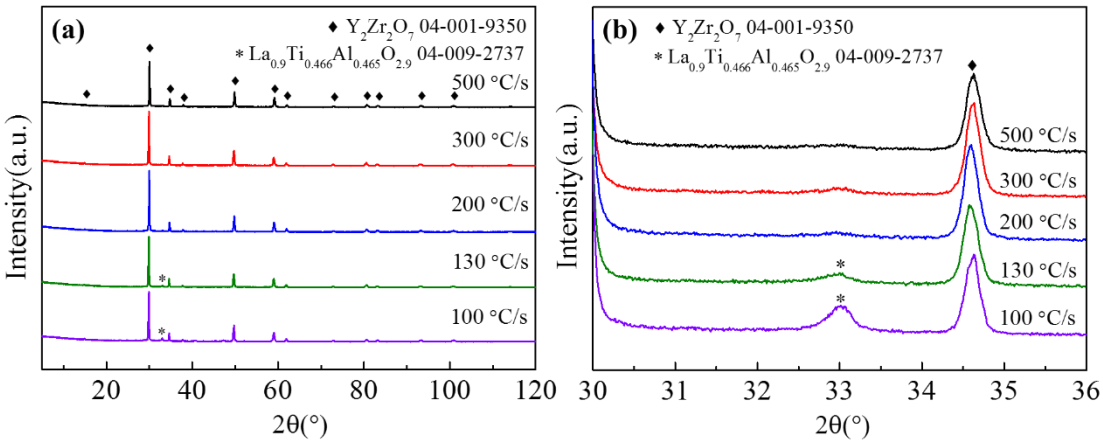

Figure 3. XRPD patterns of the as-synthesized $(La,Y)_2(Zr,Ti)_2O_7$ pyrochlore-based glass-ceramics at different cooling rates (a) and the enlargement of XRPD patterns in 30°~36° revealing the secondary crystallization evolution (b). The average cooling rates were 100 ˚C/s, 130 ˚C/s, 200 ˚C/s, 300 ˚C/s and 500 ˚C/s (free cooling), respectively.

The typical microstructure is shown in Figure 4(a). Two different phases with different greyscale contrasts are observed on the polished surface. The bright phase appears curved stripe, in which the dark phase is embedded homogenously. Both phases exhibit microscale size. Additionally, the two phases are tightly mixed and no cracks can be observed, which is interesting for further use in immobilization of high-level wastes (HLWs). Compared with previous works on pyrochlore-based glass-ceramics [16,20-21], the great difference in distribution between the crystalline pyrochlore phase and the amorphous phase in $(La,Y)_2(Zr,Ti)_2O_7$ glass-ceramics can mainly be attributed to the preparation methods. For conventional preparation methods, ample time was available for nucleation and crystal growth of pyrochlore and therefore to form the thermodynamically stable cubic structure. For rapid levitated melts solidification process, as shown in Figure 2, the sample melts solidified within 1.5 s when the cooling rate is 500 ˚C/s and the pyrochlore dendritic crystals are obtained by rapid crystal growth from the edge of the bead towards the center, which results in the curved stripe structure of pyrochlore [42]. Figure 4(b) to 4(e) shows the microstructure of samples with diameters of ~2 mm, ~3 mm, ~4mm and ~5 mm, respectively. The typical curved stripe structure of pyrochlore were observed for all sizes of samples and the two phases was homogeneity distributed. For samples with larger diameter, the stripe width of pyrochlore phase increased gradually, which is owing to the decreased solidification rate with the increase of sample size, and thus the pyrochlore phase has more time

for crystal growth.

The $(La,Y)_2(Zr,Ti)_2O_7$ pyrochlore-based glass-ceramics elaborated using a cooling rate of 500 ˚C/s (free cooling) were further studied using EDS mapping. The EDS maps of $(La,Y)_2(Zr,Ti)_2O_7$ pyrochlore-based glass-ceramics are performed to analyze the distribution of Ti, La, Zr, Y and Al at a micrometer scale, as shown in Figure 4(f). The Ti and La are homogenously distributed in the two phases. Meanwhile, the enrichment of elements occurs for Zr, Y and Al, where Zr, Y are concentrated in the bright phase and Al is concentrated in the dark phase. For the formation of pyrochlore structures, the ionic radius and valence state of elements are the most important two factors. The ionic radius of La^{3+}, Y^{3+} in 8-coordination and Zr^{4+}, Ti^{4+} in 6-coordination are 1.16 Å, 1.019 Å and 0.72 Å, 0.605 Å respectively [43]. The calculated average ratio of r_A/r_B is 1.64, which is comply with the radius requirements of 1.46-1.78 for the stable existence of pyrochlore [34]. Although Al in its trivalent state could meet the substitution requirement of $A_2B_2O_7$ in A site, the small atomic radius (0.39-0.535 Å [43]) makes it remain challenging to form a stable pyrochlore phase. Consequently, Zr and Y elements appear preferably located in the bright region and form a pyrochlore structure whereas Al is preferably located in the dark region in the amorphous phase.

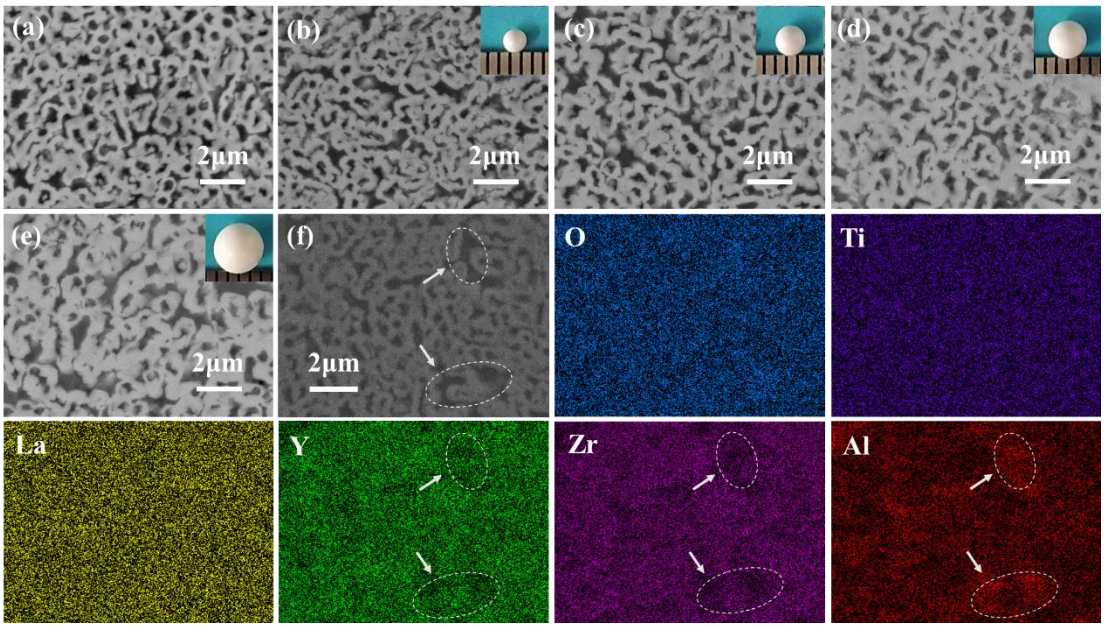

Figure 4. SEM images and corresponding EDS elemental maps of the as-synthesized $(La,Y)_2(Zr,Ti)_2O_7$ pyrochlore-based glass-ceramics. (a) Back scattering images of the polished sample with a cooling rate of 500 ˚C/s. (b-e) Back scattering images of the polished sample with

diameters of ~2 mm, ~3 mm, ~4mm and ~5 mm, respectively. (f) Secondary electron image of the polished surface and corresponding EDS maps of O, Ti, La, Zr, Y and Al.

To further study the structure of the $(La,Y)_2(Zr,Ti)_2O_7$ pyrochlore-based glass-ceramics, a nanoscale analysis was performed by Transmission Electron Microscope (TEM). Figure 5(a) confirms the coexistence of two phases, which appear interweaved with each other and tightly mixed at the nanometer scale. According to the different contrasts, two typical regions with different atom arrangements can be distinguished in the samples using high-resolution TEM mode. Some areas present a disordered atomic distribution and this amorphous character is confirmed by typical diffraction ring patterns on the FFT (Fast Fourier Transform), as shown in Figure 5(b). On the other hand, other areas show crystallographic plans characteristic of crystallized grains and the corresponding FFT patterns can be indexed with the pyrochlore structure, as shown Figure 5(c). Figure 5(d) shows an enlarged FFT pattern, indexed with the $Y_2Zr_2O_7$ pyrochlore structure along the $[0\bar{1}2]$ zone axis, showing the (242) weak reflection and the (400) strong reflection. The combination of the microstructural analyses mentioned above makes possible to define that the bright and dark regions of the as-synthesized samples correspond to pyrochlore crystalline and amorphous areas, respectively. This is in accordance with the XRPD results and suggests that $(La,Y)_2(Zr,Ti)_2O_7$ pyrochlore-based glass-ceramics are successfully synthesized in a rapid melts solidification way using aerodynamic levitator (ADL). They possess high density, i.e. no porosity, and therefore may exhibit good mechanical properties.

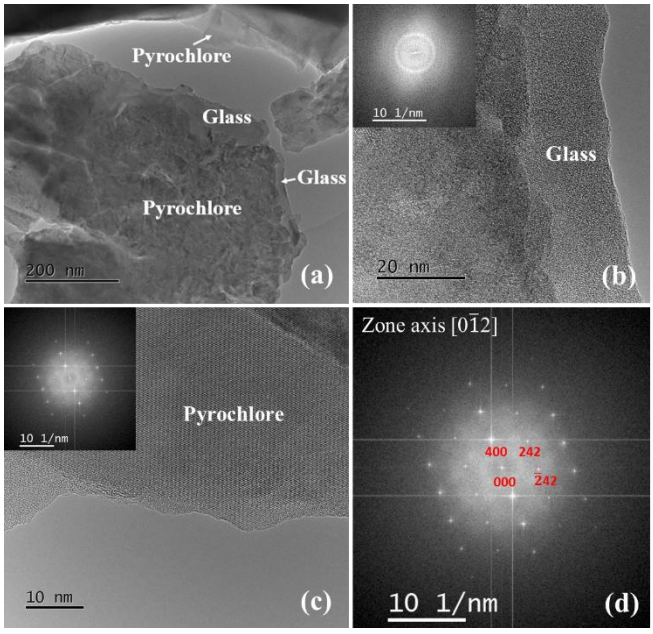

Figure 5. Transmission Electron Microscope (TEM) images and corresponding FFT patterns of the as-synthesized $(La,Y)_2(Zr,Ti)_2O_7$ pyrochlore-based glass-ceramics using a cooling rate of 500 ˚C/s. (a) Bright field image of the mixed crystalline and amorphous phases at nanoscale, (b) HRTEM image of an amorphous region (glass) with the corresponding diffraction ring FFT pattern inserted in the left corner, (c) HRTEM image of a crystalline region with the corresponding FFT pattern inserted in the left corner and (d) the previous FFT pattern enlarged and indexed by the $Y_2Zr_2O_7$ pyrochlore structure along the $[0\bar{1}2]$ zone axis.

The element distribution at the micro-scale of $(La,Y)_2(Zr,Ti)_2O_7$ pyrochlore-based glass-ceramic materials was previously characterized by EDS mappings (Figure 4). The results showed that all elements are present both in the pyrochlore and amorphous phases but their contents vary. However, due to a tightly intertwined nanometric microstructure between pyrochlore and amorphous phases, the accuracy of the EDS maps obtained by scanning electron microscopy appears limited. The quantitative analysis of the elemental distribution is challenging as some subtle composition contrasts could be hidden. Therefore, in order to quantify the composition and distribution of Al, La, Y, Zr and Ti elements, STEM-HAADF image and corresponding EDS elemental maps were acquired on the as-synthesized $(La,Y)_2(Zr,Ti)_2O_7$ pyrochlore-based glass-ceramics, as shown in Figure 6. STEM-HAADF is a Z-contrast imaging mode where the intensity is proportional to the density or to the average atomic number ($\approx Z^2$) of the phase, consequently heavier is a phase brighter it appears. The STEM-HAADF images exhibit two different phases with different contrasts, the crystalline one is brighter and the amorphous one darker. The STEM-EDS elemental maps clearly demonstrate that aluminum is present in the amorphous areas whereas Y and Zr which are located in the pyrochlore areas. Meanwhile, Ti and La appear present in both phases (amorphous and pyrochlore). Combined with the substitution requirement of A and B site in $A_2B_2O_7$, they suggest that the formed pyrochlore by rapid melts solidification is composed of La, Ti, Zr and Y, where La and Y occupy the A site and Ti and Zr are located on the B site. Aluminum and the remaining La and Ti contents are homogeneously distributed in the residual amorphous phase.

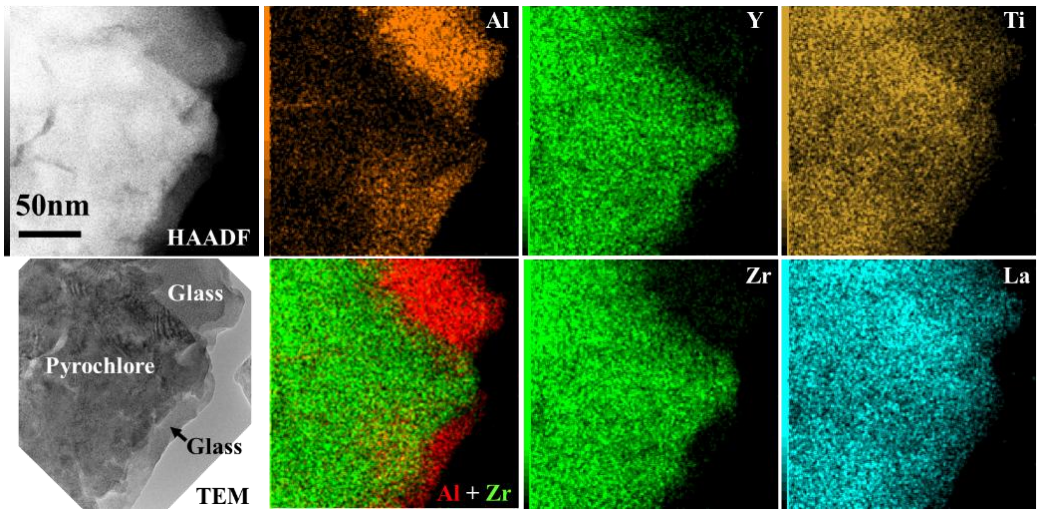

Figure 6. STEM-HAADF image and corresponding STEM-EDS cationic elemental maps of the as-synthesized $(La,Y)_2(Zr,Ti)_2O_7$ pyrochlore-based glass-ceramics at the cooling rate of 500 ˚C/s. The corresponding TEM image and the overlaid EDS maps of Al (glass) and Zr (pyrochlore).

The heat release generated by the decay of radionuclides is one of the major challenges in the immobilization of high-level wastes. Therefore, waste forms with good thermal stability are seek with great interest. Figure 7 shows the comparison of glass transition temperatures (T_g) between $(La,Y)_2(Zr,Ti)_2O_7$ pyrochlore-based glass-ceramics and some typical borosilicate glasses used for the immobilization of HLWs. The glass transition temperature of the La_2O_3-TiO_2-Al_2O_3 (LaTiAlO) amorphous phase is 863 ˚C, which is much higher than the values of the glasses currently used for actinide immobilization, such as borosilicate glasses (BSG, ~540 ˚C), alumina borosilicate glass (AlBSG, ~547 ˚C), barium borosilicate glass (BaBSG, ~512 ˚C) and lead borosilicate glass (PdBSG, ~476 ˚C) [44]. Therefore the prepared $(La,Y)_2(Zr,Ti)_2O_7$ pyrochlore-based glass-ceramics demonstrate much better thermal stability for practical applications. As shown in Table 1, the amorphous phase of the prepared glass-ceramic samples consist of La_2O_3, TiO_2 and Al_2O_3, whose molar dissociation energy is 193.9 kJ/mole, 103.9 kJ/mole and 192.0 kJ/mole, respectively. The amorphous phase of conventional glass-ceramics for nuclear waste solidification mainly consist of alkali metal oxides (<71.6 kJ/mole), SiO_2 (101.3 kJ/mole) and B_2O_3 (170.0 kJ/mole) [21,22,45]. In contrast, the La_2O_3-TiO_2-Al_2O_3 amorphous phase possesses a higher dissociation energy. Therefore, the higher glass transition temperatures may be mainly attributed to the different glass compositions and dissociation energies. Additionally, the glass transition temperature is also related to the thermal history of the material. In this work, the glass-ceramic

samples were solidified from a molten state at a relatively fast cooling rate (500 ˚C/s), which increases the glass transition temperature and thus improve the thermal stability of the amorphous phase.

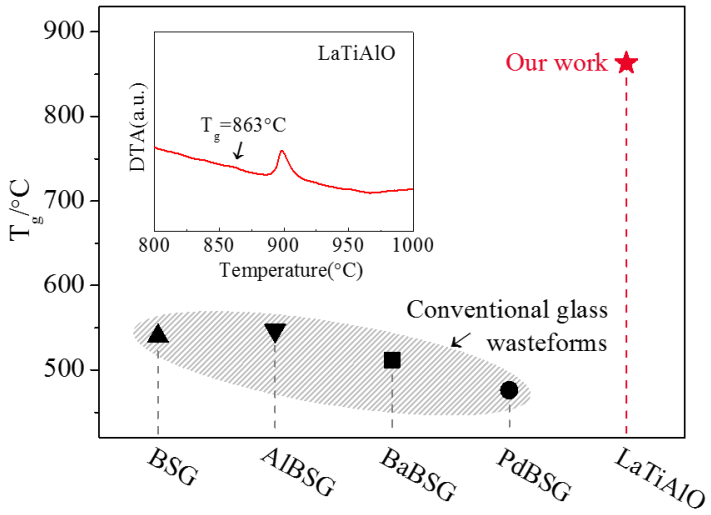

Figure 7. Comparison of glass transition temperature T_g of $(La,Y)_2(Zr,Ti)_2O_7$ pyrochlore-based glass-ceramics at the cooling rate of 500 ˚C/s and some typical borosilicate glasses used for the immobilization of HLWs [44]. The insert showed DTA curve of the as-synthesized glass-ceramics.

To demonstrate the advantages of the $(La,Y)_2(Zr,Ti)_2O_7$ pyrochlore-based glass-ceramics solidified by aerodynamic levitation, comparisons of pressure demand, reaction time and the complexity of the solidification process of samples with some typical sintering and crystallization methods of the preparation of pyrochlore-based glass-ceramics waste forms are presented in Figure 8. For a common route, glass precursors and/or pyrochlore precursors are required before reaction, which increases the preparation time, as well as the complexity of the process. Conventional sintering and crystallization methods are generally time-consuming and require high pressure, as shown in the gray region of Figure 8. Compared with the previous reports, it can be noticed that the pressure demand (room atmosphere) and reaction time (within 1.5 s, as shown in Figure 2(B)) of $(La,Y)_2(Zr,Ti)_2O_7$ pyrochlore-based glass-ceramics are drastically reduced compared to the conventional sintering and crystallization methods. The complexity of the solidification process of samples are also greatly simplified (no glass/pyrochlore precursors are required). In conclusion, the rapid melt solidification of $(La,Y)_2(Zr,Ti)_2O_7$ pyrochlore-based

glass-ceramics by aerodynamic levitation demonstrates great potential applications for the immobilization of high-level wastes.

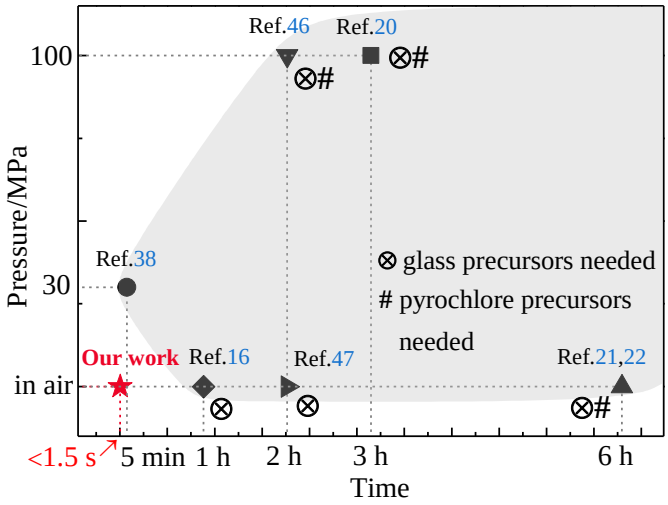

Figure 8. Pressure demand versus consolidating time during the synthesis of $(La,Y)_2(Zr,Ti)_2O_7$ pyrochlore-based glass-ceramics at the cooling rate of 500 ˚C/s via melting method together with some typical sintering and crystallization methods of the preparation of pyrochlore-based glass-ceramics waste form.

4. Conclusions

Novel $(La,Y)_2(Zr,Ti)_2O_7$ pyrochlore-based glass-ceramics were designed and successfully prepared by melt solidification process with foreseen applications for the immobilization of HLWs. The structure of the obtained glass-ceramic samples were characterized using XRPD, SEM, EDS, HRTEM and STEM-HAADF. The prepared $(La,Y)_2(Zr,Ti)_2O_7$ pyrochlore-based glass-ceramics appear dense and crack-free. The typical curved and striped structure of the glass-ceramics was owed to the rapid crystal growth from the outside towards the center of the bead during the solidification process. The thermal properties of the samples were measured by DTA. The high glass transition temperature T_g (863 ˚C) demonstrates that the obtained samples possess outstanding thermal stability compared with the conventional borosilicate glass. In summary, the rapid solidification synthesis of $(La,Y)_2(Zr,Ti)_2O_7$ pyrochlore-based glass-ceramics propose a promising path towards the immobilization of HLWs, and show great potential applications for future's nuclear waste disposal.

Acknowledgements

This work was financially supported by The National Key Research and Development

Program of China (No.2017YFC0703205), National Natural Science Foundation of China (No.51972304, No.51971208), The Project of Scientific Experiment on Chinese Manned Space Station, Chinese Academy of Sciences President's International Fellowship Initiative for 2021 (No.2021VEA0012), Innovation Academy for Green Manufacture, Chinese Academy of Sciences (No. IAGM2020C25). TEM results were realized through the project of Région-Centre Val de Loire and the French minister of research (MESRI-DRRT) and Centre-Val de Loire region with the European regional development fund (ERDF) which are cofunded by the European Union.

Author contributions

Jianqiang Li: Conceptualization, Methodology, Writing-Review & Editing, Supervision, Funding Acquisition. **Mathieu Allix**: Methodology, Resources, Writing-Review & Editing. **Yongchang Guo**: Conceptualization, Methodology, Investigation, Writing-Original Draft, Writing-Review & Editing, Supervision, Project Administration. **Ying Zhang**: Investigation, Writing-Review & Editing. **Cécile Genevois**: Investigation, Resources. **Shaowei Feng**: Investigation, Resources. **Emmanuel Véron**: Investigation, Resources. **Hong Sun**: Resources.

Declaration of interests

The authors declare that they have no known competing financial interests or personal relationships that could have appeared to influence the work reported in this paper.

Reference

[1] Radioactive waste management. Available from https://www.world-nuclear.org/information-library/nuclear-fuel-cycle/nuclear-wastes/radioactive-waste-management.aspx

[2] M.I. Ojovan, W.E. Lee, An introduction to nuclear waste immobilisation, second ed., Chatswood: Elsevier, Sydney, 2014.

[3] W.J. Weber, A. Navrotsky, S. Stefanovsky, E.R. Vance, E. Vernaz, Materials science of high-level nuclear waste immobilization, MRS Bull. 34 (2009) 46-53. https://doi.org/10.1557/mrs2009.12.

[4] A.R. Boccaccini, S. Atiq, R.W. Grimes, Hot-pressed glass matrix composites containing pyrochlore phase particles for nuclear waste encapsulation, Adv. Eng. Mater. 5 (2003) 501-508. https://doi.org/10.1002/adem.200300352.

[5] L. Wang, T.X. Liang, Ceramics for high level radioactive waste solidification, J. Adv. Ceram. 1 (2012) 194-203. https://doi.org/10.1007/s40145-012-0019-8.

[6] S.A. McMaster, R. Ram, N. Faris, M.I. Pownceby, Radionuclide disposal using the pyrochlore supergroup of minerals as a host matrix-a review, J. Hazard. Mater. 360 (2018) 257-269. https://doi.org/10.1016/j.jhazmat.2018.08.037.

[7] W.E. Lee, M.I. Ojovan, M.C. Stennett, N.C Hyatt, Immobilisation of radioactive waste in glasses, glass composite materials and ceramics, Adv. App. Ceram. 105 (2006) 3–12. https://doi.org/10.1179/174367606X81669.

[8] A. Chartier, J.P. Crocombette, C. Meis, W.J. Weber, L.R. Corrales, Radiation effects in lanthanum pyrozirconate, Nucl. Instrum. Meth. B. 250 (2006) 17–23. https://doi.org/10.1016/j.nimb.2006.04.079.

[9] M. Jafar, S.B. Phapale, B.P. Mandal, R. Mishra, A.K. Tyagi, Preparation and structure of uranium-incorporated $Gd_2Zr_2O_7$ compounds and their thermodynamic stabilities under oxidizing and reducing conditions, Inorg. Chem. 54 (2015) 9447-9457. https://doi.org/10.1021/acs.inorgchem.5b01300.

[10] H. Xu, Y. Wang, Electron energy-loss spectroscopy (EELS) study of oxidation states of Ce and U in pyrochlore and uraninite-natural analogues for Pu- and U-bearing waste forms, J. Nucl. Mater. 265 (1999) 117–123. https://doi.org/10.1016/S0022-3115(98)00566-2.

[11] R. Gieré, C. Hatcher, E. Reusser, E.C. Buck, Element partitioning in a pyrochlore based ceramic nuclear waste form, Mrs. Proc. 713 (2002) 303-310.

[12] T. Taurines, B. Boizot, Microstructure of powellite-rich glass-ceramics: a model system for high level waste immobilization, J. Am. Ceram. Soc. 95 (2012) 1105-11. https://doi.org/10.1111/j.1551-2916.2011.05015.x.

[13] A.K. Ringwood, S.E. Kesson, N.G. Ware, W. Hibberson, A. Major, Immobilisation of high level nuclear reactor wastes in synroc, Nature. 278 (1979) 219–23. https://doi.org/10.1038/278219a0.

[14] P. Loiseau, D. Caurant, Glass-ceramic nuclear waste forms obtained by crystallization of SiO_2-Al_2O_3-CaO-ZrO_2-TiO_2, glasses containing lanthanides (Ce, Nd, Eu, Gd, Yb) and actinides (Th): Study of the crystallization from the surface, J. Nucl. Mater. 402 (2010) 38–54. https://doi.org/10.1016/j.jnucmat.2010.04.021.

[15] A. K. De, B. Luckscheiter, W. Lutze, G. Malow, E. Schiewer, Development of glass-ceramics for the incorporation of fission products, Am. Ceram. Soc. Bull. 55 (1976) 500–503.

[16] Y. Zhang, Z. Zhang, G. Thorogood, E. R. Vance, Pyrochlore based glass-ceramics for the immobilization of actinide-rich nuclear wastes: from concept to reality, J. Nucl. Mater. 432 (2013) 545–547. https://doi.org/10.1016/j.jnucmat.2012.08.035.

[17] M. L. Carter, H. Li, Y. Zhang, A. L. Gillen, E. R. Vance, HIPed tailored pyrochlore-rich glass-ceramic waste forms for the immobilization of nuclear waste, Mrs. Proc. 1124 (2009) 195-206.

[18] Y. Zhang, L. Kong, I. Karatchevtseva, R. D. Aughterson, D. J. Gregg, G. Triani, Development of brannerite glass-ceramics for the immobilization of actinide-rich radioactive wastes, J. Am. Ceram. Soc. 100 (2017) 4341-4351. https://doi.org/10.1111/jace.14975.

[19] Y. Zhang, L. Kong, R. D. Aughterson, I. Karatchevtseva, R. Zheng, Phase evolution from $Ln_2Ti_2O_7$ (Ln=Y and Gd) pyrochlores to brannerites in glass with uranium incorporation, J. Am. Ceram. Soc. 100 (2017) 5535-5546. https://doi.org/10.1111/jace.15051.

[20] T. Wei, Y. Zhang, L. Kong, Y. Kim, A. Xu, I. Karatchevtseva, N. Scales, D. J. Gregg, Hot isostatically pressed $Y_2Ti_2O_7$ and $Gd_2Ti_2O_7$ pyrochlore glass-ceramics as potential waste forms for actinide immobilization, J. Eur. Ceram. Soc. 39 (2019) 1546-1554.

https://doi.org/10.1016/j.jeurceramsoc.2018.11.012.

[21] L. Kong, I. Karatchevtseva, Y. Zhang, A new method for production of glass $Ln_2Ti_2O_7$ pyrochlore (Ln=Gd, Tb, Er, Yb), J. Eur. Ceram. Soc. 37 (2017) 4963-4972. https://doi.org/10.1016/j.jeurceramsoc.2017.06.051.

[22] L. Kong, Y. Zhang, I. Karatchevtseva, Preparation of $Y_2Ti_2O_7$ pyrochlore glass-ceramics as potential waste forms for actinides: the effects of processing conditions, J. Nucl. Mater. 494 (2017) 29-36. https://doi.org/10.1016/j.jnucmat.2017.07.004.

[23] P. Loiseau, D. Caurant, N. Baffier, L. Mazerolles, C. Fillet, Glass–ceramic nuclear waste forms obtained from SiO_2-Al_2O_3-CaO-ZrO_2-TiO_2 glasses containing lanthanides (Ce, Nd, Eu, Gd, Yb) and actinides (Th): study of internal crystallization, J. Nucl. Mater. 335 (2004) 14-32. https://doi.org/10.1016/j.jnucmat.2004.05.020.

[24] D. Caurant, O. Majerus, P. Loiseau, I. Bardez, N. Baffier, J. L. Dussossoy, Crystallization of neodymium-rich phases in silicate glasses developed for nuclear waste immobilization, J. Nucl. Mater. 354 (2006) 143-162. https://doi.org/10.1016/j.jnucmat.2006.03.014.

[25] Y. Zhang, I. Karatchevtseva, L. Kong, T. Wei, Z. Zhang, Structural and spectroscopic studies on the crystallization of uranium brannerite phases in glass, J. Am. Ceram. Soc. 101 (2018) 5219-5228. https://doi.org/10.1111/jace.15750.

[26] M. Jafar, S.N. Achary, N.P. Salke, A.K. Sahu, R. Rao, A.K. Tyagi, X-ray diffraction and Raman spectroscopic investigations on $CaZrTi_2O_7$-$Y_2Ti_2O_7$ system: delineation of phase fields consisting of potential ceramic host materials, J. Nucl. Mater. 475 (2016) 192-199. https://doi.org/10.1016/j.jnucmat.2016.04.016.

[27] M. Jafar, P. Sengupta, S.N. Achary, A.K. Tyagi, Phase evolution and microstructural studies in $CaZrTi_2O_7$-$Nd_2Ti_2O_7$ system, J. Am. Ceram. Soc. 97 (2014) 609-616. https://doi.org/10.1111/jace.12664.

[28] B.P. Mandal, M. Pandey, A.K. Tyagi, $Gd_2Zr_2O_7$ pyrochlore: potential host matrix for some constituents of thoria based reactor's waste, J. Nucl. Mater. 406 (2010) 238-243. https://doi.org/10.1016/j.jnucmat.2010.08.042.

[29] K.V.G. Kutty, R. Asuvathraman, R.R. Madhavan, H. Jena, Actinide immobilization in crystalline matrix: a study of uranium incorporation in gadolinium zirconate, J. Phys. Chem.

Solids. 66 (2005) 596-601. https://doi.org/10.1016/j.jpcs.2004.06.066.

[30] J.P. Icenhower, D.M. Strachan, B.P. McGrail, R.D. Scheele, E.A. Rodriquez, L.J. Steel, V.L. Legore, Dissolution kinetics of pyrochlore ceramics for the disposition of plutonium, Am. Mineral. 91 (2006) 39-53. https://doi.org/10.2138/am.2006.1709.

[31] D.M. Strachan, R.D. Scheele, E.C. Buck, J.P. Icenhower, A.E. Kozelisky, R.L. Sell, R.J. Elovich, W.C. Buchmiller, Radiation damage effects in candidate titanates for Pu disposition: Pyrochlore, J. Nucl. Mater. 345 (2005) 109-135. https://doi.org/10.1016/j.jnucmat.2005.04.064.

[32] M. James, M.L. Carter, Z. Zhang, Y. Zhang, K.S. Wallwork, M. Avdeev, Crystal chemistry and structures of (Ca, U) titanate pyrochlores, J. Am. Ceram. Soc. 93 (2010) 3464-3473. https://doi.org/10.1111/j.1551-2916.2010.03871.x.

[33] M.L. Carter, H. Li, Y. Zhang, E.R. Vance, D.R.G. Mitchell, Titanate ceramics for immobilization of uranium-rich radioactive wastes arising from 99Mo production, J. Nucl. Mater. 384 (2009) 322-326. https://doi.org/10.1016/j.jnucmat.2008.12.042.

[34] M.A. Subramanian, G.A. Ravamudan, G.V.S. Rao, Oxide pyrochlores-a review, Prog. Solid. State. Chem. 15 (1983) 55-143. https://doi.org/10.1016/0079-6786(83)90001-8.

[35] A.R. Boccaccini, E. Bernardo, L. Blain, N.D. Boccaccini, Borosilicate and lead silicate glass matrix composites containing pyrochlore phases for nuclear waste encapsulation, J. Nucl. Mater. 327 (2004) 148-158. https://doi.org/10.1016/j.jnucmat.2004.01.019.

[36] E.R. Aluri, A.P. Grosvenor, A study of the electronic structure and structural stability of $Gd_2Ti_2O_7$ based glass-ceramic composites, RSC Adv. 5 (2015) 80939-80949. https://doi.org/10.1039/c5ra10720b.

[37] L. Zhou, F. Li, J.X. Liu, High-entropy $A_2B_2O_7$-type oxide ceramics: A potential immobilising matrix for high-level radioactive waste, J. Hazard. Mater. 415 (2021) 125596. https://doi.org/10.1016/j.jhazmat.2021.125596.

[38] X.Y. Shu, S.Z. Chen, X.R. Lu, Rapid synthesis of $Gd_2Zr_2O_7$ glass-ceramics using spark plasma sintering, J. Am. Ceram. Soc. 103 (2020) 597-603. https://doi.org/10.1111/jace.16658.

[39] Y.C. Guo, J.Q. Li, Y. Zhang, S.W. Feng, H. Sun, High-entropy R_2O_3-Y_2O_3-TiO_2-ZrO_2-Al_2O_3 glasses with ultrahigh hardness, Young's modulus, and indentation fracture toughness, iScience. (2021) 102735.

https://doi.org/10.1016/j.isci.2021.102735.

[40] X.Y. Li, J.Y. Li, J.Q. Li, Upconversion $32Nb_2O_5$-$10La_2O_3$-$16ZrO_2$ glass activated with Er^{3+}/Yb^{3+} and dye sensitized solar cell application, J. Adv. Ceram. 6 (2017) 312-319. https://doi.org/10.1007/s40145-017-0243-3.

[41] J.T. Fan, V. Sarou-Kanian, X.Y. Yang, et al, $La_2Ga_3O_{7.5}$: a metastable ternary melilite with a super-excess of inter-stitial oxide ions synthesized by direct crystallization of the melt, Chem. Mater. 32 (2020) 9016-9025. https://doi.org/10.1021/acs.chemmater.0c03441.

[42] W. Wisniewski, P. Vanárek, A. Prnová, et al, Y_2O_3-Al_2O_3 microsphere crystallization analyzed by electron backscatter diffraction (EBSD), Sci. Rep. 10 (2020). https://doi.org/10.1038/s41598-020-67816-7.

[43] R.D. Shannon, C.T. Prewitt, Effective ionic radii in oxides and fluorides, Acta Cryst. B25 (1969) 925-946. https://doi.org/10.1107/S0567740869003220.

[44] B.K. Maji, H. Jena, R. Asuvathraman, Electrical conductivity and glass transition temperature (T_g) measurements on some selected glasses used for nuclear waste immobilization, J. Non-Cryst. Solids. 434 (2016) 102-107. https://doi.org/10.1016/j.jnoncrysol.2015.12.008.

[45] A. Makishima, J.D. Mackenzie, Direct calculation of Young's modulus of glass, J. Non-Cryst. Solids. 12 (1973) 35-45. https://doi.org/10.1016/0022-3093(73)90053-7.

[46] Y.J. Zhang, Z.M. Zhang, T. Wei, Pyrochlore glass-ceramics fabricated via both sintering and hot isostatic pressing for minor actinide immobilization, J. Am. Ceram. Soc. 103 (2020) 5470-5479. https://doi.org/10.1111/jace.17119.

[47] Z.Q. Feng, H. Xie, L.L. Wang, Glass-ceramics with internally crystallized pyrochlore for the immobilization of uranium wastes, Ceram. Int. 45 (2019) 16999-17005. https://doi.org/10.1016/j.ceramint.2019.05.249.